



A new analytically modified embedded discrete fracture model for pressure transient analysis in fluid flow

Biao Zhou^a, Zhiming Chen^{a,*}, Zhigang Song^a, Zekai Tang^a, Bin Wang^a, Olufemi Olorode^b

^a National Key Laboratory of Petroleum Resources and Engineering, China University of Petroleum (Beijing), China

^b Craft and Hawkins Department of Petroleum Engineering, Louisiana State University, Baton Rouge, LA, USA

ARTICLE INFO

Keywords:

Embedded discrete fracture model
Analytical modification
Fractured porous media
Pressure transient analysis
Fluid flow

ABSTRACT

In the past few decades, multi-stage hydraulic fracturing has emerged as a crucial technology for the commercial development of unconventional oil and gas (UOG) resources. It is crucial to accurately and efficiently characterize transient fluid flow near fractures, which is a critical concern for many researchers. Discrete fracture models (DFMs) are primarily used to analyze the pressure transient behaviors of fluid flow in naturally fractured porous media. DFMs can accurately capture transient fluid flow near fractures, but they require a substantial number of grids to ensure computational accuracy, leading to higher computational costs. On the other hand, standard embedded discrete fracture models (EDFMs) based on pseudo-steady-state assumptions are computationally efficient, but they struggle to model the early transient fluid flow near fractures accurately. To address this limitation, we propose a new analytically modified EDFM (AEDFM) with structured Cartesian grids for analyzing the pressure transient behaviors of fluid flow in naturally fractured porous media.

The transmissibility between the matrix and fractures is adjusted by multiplying it with a transient factor. In addition, we have validated the accuracy and efficiency of our proposed model through comparisons with results from analytical models and a standard well-testing software package. The results demonstrate the significance of our proposed model in accurately capturing transient fluid flow around fractures and reducing computational costs. In this work, we analyze the pressure transient behaviors of fluid flow using various parameter values and further evaluate the significance of the proposed modifications. The results indicate that AEDFM can effectively match the early nonlinear pressure drop near fractures compared to the standard EDFM. This work presents a powerful tool for the fast and accurate analysis of pressure transient behaviors of fluid flow in naturally fractured porous media.

1. Introduction

In the past few decades, the estimated ultimate recovery (EUR) of production wells has been significantly enhanced by applying hydraulic fracturing technology (Wu et al., 2017). Hydraulic fracturing has emerged as a crucial technology for commercially developing unconventional oil and gas (UOG) resources. Scholars have developed various mathematical models, both continuum and discrete, to characterize fluid flow within and around fractures due to their significant contribution to fluid flow in fractured porous media (Chen and Yu, 2022; Karimi-Fard and Firoozabadi, 2001; Kazemi et al., 1976; Li and Lee, 2008; Wan and Aziz, 1999; Warren and Root, 1963). Well-test models based on these approaches are essential for pressure transient analysis (PTA) and evaluation of fracture parameters (Chandra et al., 2013).

These models require high computational accuracy and solve pressure responses at scales of several seconds or smaller.

Continuum models represent the fractured porous media as a continuous medium with homogeneous properties. These models include the dual-permeability, dual-porosity, and multiple continuum models (Gilman and Kazemi, 1983; Pruess and Wu, 1993; Warren and Root, 1963). The dual-porosity model was first proposed by Barenblatt (Barenblatt et al., 1960). Warren and Root (1963) proposed the dual-porosity model known as the Warren and Root model, which is the most commonly used model in the pressure transient analysis of fluid flow in fractured porous media. The transfer term between the matrix and fractures in this model is derived based on a pseudo-steady-state assumption. Later, Dean and Lo (1988) proposed the dual-permeability model as an alternative to the dual-porosity model. The

* Corresponding author.

E-mail address: zhimingchn@cup.edu.cn (Z. Chen).

<https://doi.org/10.1016/j.jhydrol.2024.131330>

Received 25 November 2023; Received in revised form 1 April 2024; Accepted 30 April 2024

Available online 12 May 2024

0022-1694/© 2024 Elsevier B.V. All rights are reserved, including those for text and data mining, AI training, and similar technologies.

dual-permeability model assumes that the matrix has both storage capacity and flow capacity. However, it is important to note that this model is based on the pseudo-steady-state assumption, and the transfer term derived from this assumption is only applicable at late times. To address this limitation, Zimmerman et al. (1993) employed a nonlinear equation to derive the transient transfer term between the matrix and fractures. This approach enables a more precise simulation of the flux between the matrix and fractures across all time scales, including early and late stages. Azom and Javadpour (2012) later suggested that the transient transfer term between the matrix and fractures could be expressed as a product of the pseudo-steady-state transfer term and a transient factor. Besides, Pruess and Narasimhan (1985) developed a multiple interacting continua (MINC) model, which is an extension of the dual-porosity model. However, continuum medium models struggle to accurately represent the complex geometry of fractures, as they assume the matrix is uniformly divided by them (Egya et al., 2019; Kuchuk and Biryukov, 2014).

In contrast to continuum models, discrete models represent each fracture in the porous media individually. This is achieved by considering fractures as $n-1$ dimensional objects in an n -dimensional model (Kim and Deo, 2000). As a result, the fluid flow in the porous media can be modeled more accurately. Discrete models mainly include the discrete fracture model (DFM) and the embedded discrete fracture model (EDFM). In DFM, fractures are positioned at the interfaces between neighboring matrix grids by using unstructured grids such as triangular/tetrahedral and perpendicular bisector (PEBI) grids (Karimi-Fard and Firoozabadi, 2003; Sandve et al., 2012). The fractures are meshed in this way to ensure a clear and logical structure of the model. Furthermore, the use of unstructured grids enables easy implementation of local grid refinement around fractures, allowing the DFM to accurately capture the transient fluid flow around them (Jiang and Younis, 2015; Zhao et al., 2018). However, this approach inevitably comes with a very high computational cost. To address this limitation, Lee et al. (2001) developed the embedded discrete fracture model (EDFM), which constructs matrix and fracture grids independently. The flux between each fracture and its host matrix grid is calculated using a non-neighboring connection (NNC) flux term (Xu, 2015). The EDFM method has been widely applied in simulating fluid flow in fractured porous media (Moinfar et al., 2013; Wang and Fidelibus, 2021; Yu et al., 2017; Yu et al., 2019; Cao et al., 2023; Hu et al., 2023; Zhao et al., 2023). However, like the pseudo-steady state transfer term in the dual-permeability model, this NNC flux term is derived based on the pseudo-steady state assumption and is linearly related to pressure. Olorode and Rashid (2022) later introduced the transient embedded discrete fracture model (tEDFM) to address the nonlinear pressure drop associated with early-time transient fluid flow between the matrix and fractures. This work provides new insights to address the limitations of EDFM in dealing with transient fluid flow. Additionally, Tene et al. (2017) developed the projection-based embedded discrete fracture model (pEDFM) based on the EDFM, which can effectively handle flow barriers such as faults, a limitation of EDFM. Subsequently, Olorode et al. (2020) proposed a robust 3D pEDFM algorithm. Furthermore, Rashid and Olorode (2023) noted that pEDFM is unable to accurately simulate low-conductivity fractures that are neither aligned with the simulation grid nor intersect diagonals of the matrix cell. To address this limitation of the pEDFM model, they developed the continuous projected-based EDFM (CPEDFM). DFM and EDFM are both powerful tools for the numerical simulation of fluid flow in fractured porous media.

DFM is widely used in numerical well-test models for pressure transient analysis of fluid flow. For example, Liu et al. (2020) proposed a numerical well-test model for the pressure transient analysis of fluid flow with discretely distributed natural fractures using the DFM method and PEBI grids. Chen et al. (2023) studied the pressure transient behaviors of two multi-fractured horizontal wells (MFHWs) with well interference and two-phase flow using the DFM method and PEBI grids.

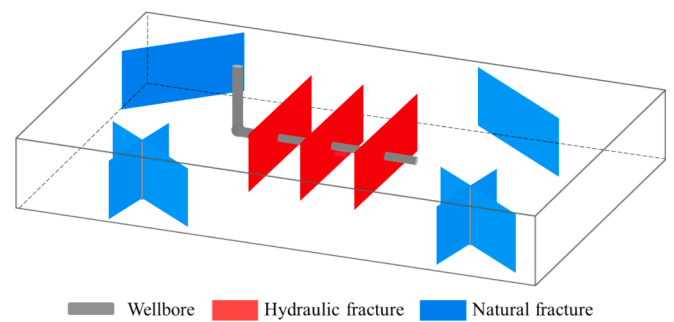


Fig. 1. Schematic diagram of the physical model of an MFHW in the naturally fractured porous media.

Furthermore, EDFM has been used by some researchers for pressure transient analysis of fluid flow. Liu et al. (2022) proposed a hybrid discrete fracture method that uses DFM and locally refined unstructured grids to simulate hydraulic fractures, while natural fractures are modeled using EDFM. Later, Xu and Sepehrnoori (2022) combined EDFM with nested local grid refinement to accurately capture transient fluid flow around fractures. However, this approach requires sufficiently fine grids around fractures, leading to a relatively large number of grids. Xiang et al. (2023) investigated the pressure transient behaviors of fractured wells considering gas-water two-phase flow using EDFM and unstructured PEBI grids. However, there is still a lack of a numerical well-test model that is accurate and efficient for pressure transient analysis of fluid flow.

In this work, we develop a new analytically-modified EDFM (AEDFM) with structured Cartesian grids to accurately and efficiently analyze the pressure transient behaviors of fluid flow in naturally fractured porous media. Firstly, the transmissibility between the fracture and its host matrix grids in the EDFM method was modified to model the transient fluid flow between the matrix and fractures. Then, the flow rate from the fracture into the wellbore was treated as a separate variable to eliminate the error associated with the equivalent radius based on pseudo-steady-state assumptions. This model's accuracy was verified by comparing it with the analytical model and a specialized commercial software package for pressure transient analysis. Additionally, we discussed the limitations of standard EDFM at early times. To demonstrate the accuracy advantages of AEDFM, we compared its results with those of EDFM and tEDFM. Finally, we investigated the impact of parameters related to natural fractures on the pressure transient behaviors of fluid flow. This paper presents a powerful tool for the pressure-transient analysis of fluid flow in naturally fractured porous media.

2. Analytically modified embedded discrete model

2.1. Physical model

Fig. 1 shows a multi-stage fractured horizontal well (MFHW) located in the center of a naturally fractured porous media with closed boundaries. To develop the mathematical model, several assumptions are made:

- The porous media is assumed to be homogeneous, isotropic, and characterized by uniform initial pressure and temperature.
- The system is assumed to be isothermal, so temperature is excluded from consideration.
- The flow fluid is a single-phase, slightly compressible fluid that follows Darcy's law.
- The fractures fully penetrated the porous media, and fluid flows into the wellbore only through hydraulic fractures.
- There are no natural fractures are present within 30 m of the hydraulic fractures.

- The wellbore storage and skin effects are taken into consideration.
- The production well produces at a constant rate.

2.2. Mathematical model

2.2.1. Matrix flow equation

The mass conservation equation for fluid flow in the matrix can be written as:

$$24 \frac{\partial(\rho\phi_m)}{\partial t} + \nabla \cdot (\rho \vec{v}_m) - \rho(q_m - q_{m,f})/V = 0 \quad (1)$$

where 24 is a coefficient used for unit conversion; ρ is the density of the fluid, kg/m³; ϕ_m is the matrix porosity, fraction; t is the production time, h; \vec{v}_m is the Darcy velocities of the fluid in the matrix, m/d; q_m is the source/sink term in the matrix, m³/d; $q_{m,f}$ is the transfer function of the fluid flow from the matrix to the fracture, m³/d; V is the bulk volume, m³.

The Darcy velocities in Eqs.1 can be defined as:

$$\vec{v}_m = -86.4 \frac{k_m}{\mu} (\nabla p - \rho g \nabla z) \quad (2)$$

where 86.4 is a coefficient used for unit conversion; k_m is the matrix permeability, D; μ is the fluid viscosity, mPa·s; p is the pressure of the fluid, MPa; g is the gravitational acceleration; and z is the height, m.

2.2.2. Fracture flow equation

The EDFM method couples the fluid flow in the fracture cell with that in the matrix cell using non-neighboring connections (NNCs). This is achieved by incorporating a flux term into the semi-discrete form of the governing equation. The mass conservation equation for fluid flow in the fracture system can be written as:

$$24 \frac{\partial(\rho\phi_f)}{\partial t} + \nabla \cdot (\rho \vec{v}_f) - \rho(q_f - q_{f,m} - q_{f,f_2})/V = 0 \quad (3)$$

where ϕ_f is the fracture porosity, fraction; \vec{v}_f is the Darcy velocities of the fluid in the fracture, m/d; q_f is the source/sink term in the fracture, m³/d; $q_{f,m}$ is the transfer function of the fluid flow from the fracture to the matrix, m³/d; q_{f,f_2} is the transfer function of the fluid from fracture cell 1 to fracture cell 2, m³/d.

2.2.3. Wellbore equation

Usually, the effective well index (WI) is employed to calculate the flow rate between a fracture cell and a well (Peaceman, 1983), and it can be expressed as follows:

$$WI = \frac{2\pi k_f w_f}{\ln(r_e/r_w) + S} \quad (4)$$

$$q = \frac{WI}{\mu} (p - p_{wf}) \quad (5)$$

where k_f is the fracture permeability, D; w_f is the fracture aperture, m; r_e is the equivalent radius, m; r_w is the wellbore radius, m; S is the skin factor (dimensionless), and p_{wf} is the bottom-hole pressure, MPa.

The use of this approach in EDFM may result in errors in the early-stage pressure transient behaviors of fluid flow. This is because the derivation of the well index under steady-state conditions leads to excessive flow resistance in the early stage and renders it unsuitable for transient pressure computation. Considering the wellbore storage effect, we treat the flow rate into the wellbore from fractures as a variable. Based on the work of Al-Kobaisi et al. (2006), the wellbore equation can be expressed as follows:

$$24 \frac{\partial(\rho\phi_f)}{\partial t} + \nabla \cdot (\rho \vec{v}_f) - \rho(q_f - q_{f,m} - q_{f,f_2})/V + Q/V = 0 \quad (6)$$

$$Q = q_c + 24C \frac{\partial p_{wf}}{\partial t} \quad (7)$$

where Q is the well production rate, m³/d; q_c is the flow rate into the wellbore from fracture cell under the influence of wellbore storage effect, m³/d; and C is the wellbore storage coefficient, m³/MPa.

An initial value of q_c is assumed to be equal to Q . The discretized equation is then iteratively solved using Eq. (7) to obtain the variable p_{wf} and the variable q_c under the influence of the wellbore storage effect.

2.3. Numerical solution

To solve the flow equations numerically, time is discretized using the backward Euler scheme. Then, we discretize the flux terms in space using the finite volume method with a two-point flux approximation, as discussed in Section 4.4 of the MRST book (Lie, 2019). The discretized forms of Eqs. (1), (3), (6), and (7) are obtained by using the divergence operator (div) and gradient operator (grad) mentioned in this book:

$$24 \frac{[(\rho\phi_m)^{n+1} - (\rho\phi_m)^n]}{\Delta t} + \text{div}(\rho \vec{v}_m)^{n+1} - (\rho q_m)^{n+1}/V + q_m^{nnc}/V = R_m^{n+1} \quad (8)$$

$$24 \frac{[(\rho\phi_f)^{n+1} - (\rho\phi_f)^n]}{\Delta t} + \text{div}(\rho \vec{v}_f)^{n+1} - (\rho q_f)^{n+1}/V + q_f^{nnc}/V = R_f^{n+1} \quad (9)$$

$$24 \frac{[(\rho\phi_f)^{n+1} - (\rho\phi_f)^n]}{\Delta t} + \text{div}(\rho \vec{v}_f)^{n+1} - (\rho q_f)^{n+1}/V + q_f^{nnc}/V + \left(q_c^{n+1} + C \frac{p_{wf}^{n+1} - p_{wf}^n}{\Delta t} \right) / V = R_w^{n+1} \quad (10)$$

where

$$\vec{v}_\alpha = -86.4 T_{ij} \frac{k_\alpha}{\mu} [\text{grad}(p_\alpha^{n+1}) - \rho g \cdot \text{grad}(z)], \quad T_{ij} = \frac{T_{ij} \cdot T_{ji}}{T_{ij} + T_{ji}}, \quad T_{ij} = A_{ij} k_i \frac{\vec{c}_{ij} \cdot \vec{n}_{ij}}{|\vec{c}_{ij}|} \quad (11)$$

and

$$q_\alpha^{nnc} = \sum_{N=1}^{N_{nnc}} T^{nnc} \rho [(p_\alpha - \rho g z) - (p_\alpha - \rho g z)_N]^{nnc}, \quad T^{nnc} = \frac{k^{nnc} A^{nnc}}{d^{nnc}} \quad (12)$$

For matrix-fracture connections, the expressions for k^{nnc} , A^{nnc} , and d^{nnc} can be written as follows:

$$A^{nnc} = 2A_f, \quad k^{nnc} = \frac{k_m k_f}{k_m + k_f}, \quad d^{nnc} = \frac{\int_V x_n dv}{V} \quad (13)$$

where the superscript $n + 1$ represents the current time step, while the superscript n represents the previous time step; R is the residual, kg⁻¹m⁻³s⁻¹; the subscript α represents either m or f ; T_{ij} is the transmissibility factor between cell i and j , m²; A_{ij} is the face areas, m²; \vec{c}_{ij} is the vector from the centroid of cell i to the centroid of the interface of cell i and cell j ; \vec{n}_{ij} is the outward unit vector that points from the centroid of the interface to the cell j ; q^{nnc} is the mass rate exchanged through NNC, kg/d; The subscript N is a number ranging from 1 to N_{nnc} ; N_{nnc} is the total number of non-neighboring connections for each cell; A_f

Table 1
Parameters related to model verification.

		Case I	Case II	
Types	Parameters	Value		Unit
Porous media	Initial pressure	40	40	MPa
	Matrix porosity	0.1	0.1	/
	Total compressibility	5.58×10^{-4}	5.58×10^{-4}	MPa ⁻¹
	Matrix permeability	1×10^{-3}	1×10^{-3}	D
	Formation size	500×500	500×500	m
Hydraulic fracture	Fracture conductivity	100	100	mD-m
	Fracture half length	30	30	m
	Fracture height	20	20	m
	Fracture porosity	0.9	0.9	/
	Fracture width	1×10^{-2}	1×10^{-2}	m
Natural fracture	Fracture conductivity	/	50	mD-m
	Average length	/	110	m
	Fracture height	/	20	m
	Fracture porosity	/	0.5	/
	Fracture width	/	1×10^{-2}	m
Well	Fracture number	/	6	/
	Well production rate	10	10	m ³ /d
	Skin factor	2×10^{-2}	2×10^{-2}	/
	Wellbore storage coefficient	1×10^{-3}	1×10^{-3}	m ³ /MPa

is the fracture area, m²; x_n is the normal distance of the element from the fracture. Additional details on the expressions for the three types of non-neighboring connections in EDFM can be found in the work of Moinfar et al. (2013).

Olorode and Rashid (2022) suggest that the q^{nnc} term in Eqs. (8)–(10) is a linear function of the flow potential difference between matrix and fracture cells. This is the primary reason why the standard EDFM cannot match early transient fluid flow behaviors. Furthermore, drawing inspiration from the dual-porosity model to handle matrix/fracture flow, they proposed a method called tEDFM. This method corrects the matrix/fracture connection (NNC) flux in EDFM by multiplying it with a transient factor.

$$q_{\alpha,T}^{nnc} = T_f \sum_{N=1}^{N_{nnc}} T^{nnc} \rho \frac{[(p_\alpha - \rho g z) - (p_\alpha - \rho g z)_N]^{nnc}}{\mu} \quad (14)$$

$$T_f = \frac{2\Phi_i - (\Phi_m + \Phi_f)}{2(\Phi_i - \Phi_m)} \quad (15)$$

$$\Phi = p - \rho g z \quad (16)$$

where Φ is the flow potentials; the subscript i represents the initial state.

Although their research effectively matched early transient fluid flow behaviors, it still does not accurately capture early pressure transient behaviors, specifically with regard to the behaviors of the pressure

derivative plot. Pruess and Wu (1993) proposed a more accurate method for handling fracture/matrix flow in dual-porosity models using an integral method proposed by Vinsome and Westerveld (1980). The pressure distribution in the matrix cell can be approximated as follows:

$$P_m(x_m, t) = p_i + (p_f - p_i + rz_m + sx_m^2) e^{-x_m/\delta}, \quad \delta = (k_m t / 4\phi_m \mu C_t)^{1/2} \quad (17)$$

where x_m is the distance from the point in the matrix cell to the outer boundary, m; r and s are coefficients that satisfy the integration conditions; C_t is the total compressibility, MPa⁻¹.

Building on these foundations, Zimmerman et al. (1993) utilized the method proposed by Vermeulen (1953) to calculate step function pressure responses across all scales:

$$\frac{p_m - p_i}{p_f - p_i} = [1 - \exp(-\pi^2 k_m t / \phi_m \mu C_t a_m^2)]^{1/2} \quad (18)$$

where a_m is the half length of the matrix grid, m.

The transient factor has been further corrected by substituting Eq. (18) into Eq. (17), resulting in:

$$T_f = \frac{1}{2} + \frac{1}{2} [1 - \exp(-\pi^2 k_m t / \phi_m \mu C_t a_m^2)]^{1/2} \quad (19)$$

Then, Eq. (19) and Eq. (14) (instead of Eq. (12)) are substituted into the discretized equations in Eqs. (8)–(10). Finally, we have implemented our modifications in the “shale” module (<https://github.com/UnconVRs/shale>), which is one of the modules in the open-source numerical simulator MRST (Lie and Møyner, 2021), and solved for transient pressure using Newton-Raphson iteration. Next, we discuss the validation and application of AEDFM, respectively.

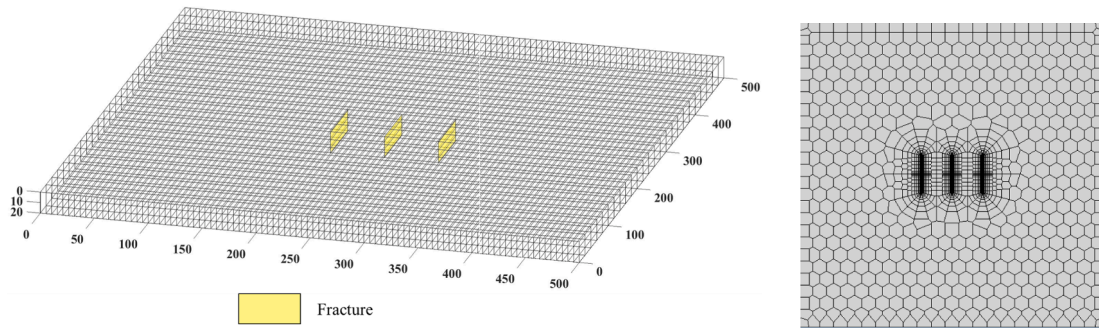
2.4. Model verification

In this section, we validate the accuracy of the proposed model by comparing it with an analytical model and a standard well-testing software package called KAPPA (with an educational license) (Houze et al., 2008). The numerical model of KAPPA adopts DFM and unstructured grids with local grid refinement. Table 1 shows the basic parameters that are used for model verification.

2.4.1. Case I: Without natural fractures

Fig. 2a shows the structured Cartesian grid ($100 \times 25 \times 1$) of the proposed model used for model verification.

We plot the results in dimensionless form to facilitate the wider application of well-test curves (Chen and Yu, 2022). The dimensionless time can be expressed as follows:



(a) Structured Cartesian Grids.

(b) Unstructured grids in KAPPA.

Fig. 2. Schematic of grids used for model verification.

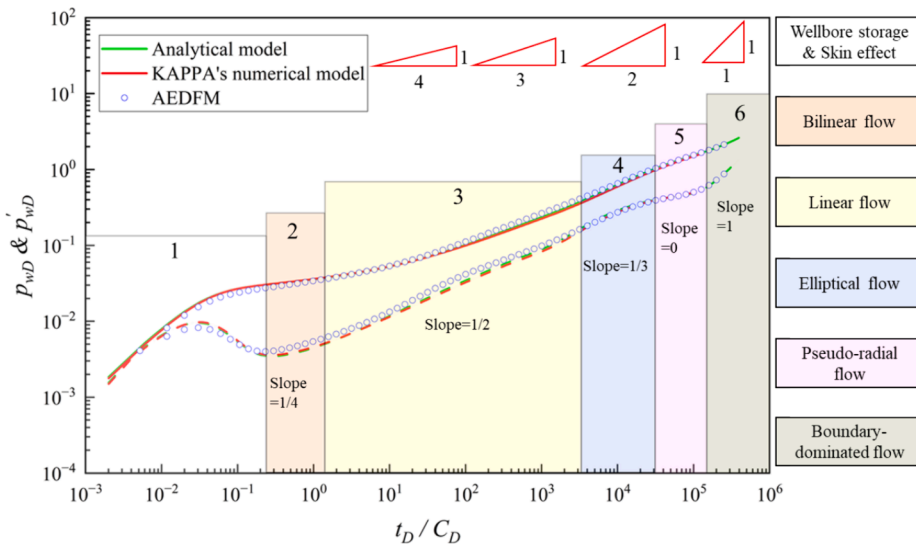


Fig. 3. Comparison between AEDFM and the analytical model, as well as KAPPA's numerical model of Case I.

Table 2
Comparison of computational time.

Types	The KAPPA's model	AEDFM (X25)	AEDFM (X50)	AEDFM (X100)
CPU	Core i7-11700	Core i7-11700	Core i7-11700	Core i7-11700
Grid number	3265	634	1259	2509
Average computational time for five times	6.1 s	2.5 s	2.7 s	3.6 s

$$t_D = \frac{3.6k_m t}{\phi_m \mu C_t X_f^2} \quad (20)$$

where X_f is the fracture half length, m.

The dimensionless wellbore storage coefficient can be written as:

$$C_D = \frac{0.1592C}{\phi_m h C_t X_f^2} \quad (21)$$

Subsequently, the dimensionless pressure can be expressed as:

$$p_D = \frac{k_m h (p_i - p)}{1.842 \times 10^{-3} q \mu B} \quad (22)$$

The result of KAPPA's numerical model is used as a reference solution p_{ref} . The L^2 absolute error between the pressure p_{AEDFM} of AEDFM and the reference solution p_{ref} is defined as follows (Zhan et al., 2023):

$$RE = \sqrt{\frac{\sum_{i=1}^n (p_{AEDFM,i} - p_{ref,i})^2}{\sum_{i=1}^n p_{ref,i}^2}} \quad (23)$$

where n is the number of time steps.

The model comparison results are presented in Fig. 3. The double logarithmic curves in Fig. 3 show that the dimensionless pressure and pressure derivative of AEDFM also closely match those of the analytical model and KAPPA's model. Furthermore, as seen in Table 2, the AEDFM model uses only 2509 grid blocks and takes only 3.6 s to compute the results over 70-time steps. The time step for KAPPA's model is the same as that for the AEDFM. Compared to the results obtained from KAPPA, our model can significantly reduce computational costs while ensuring high accuracy. Additionally, the fluid flow stages of the MFHW can be divided into six stages: wellbore storage and skin effects, bilinear flow,

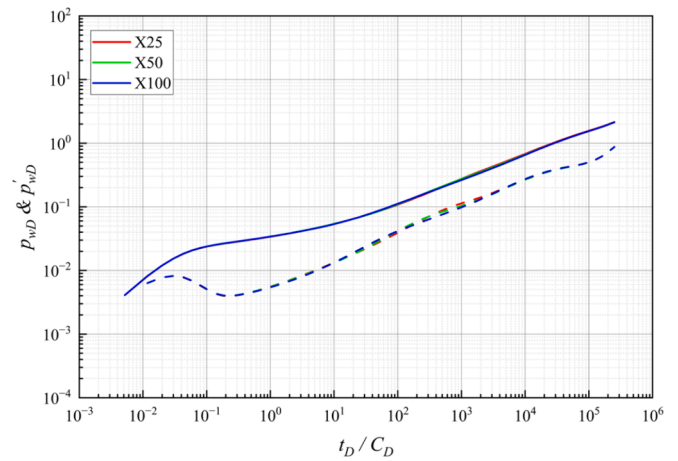


Fig. 4. Comparison of results for different grid numbers. X25, X50, and X100 denote 25, 50, and 100 grids in the x-direction, respectively.

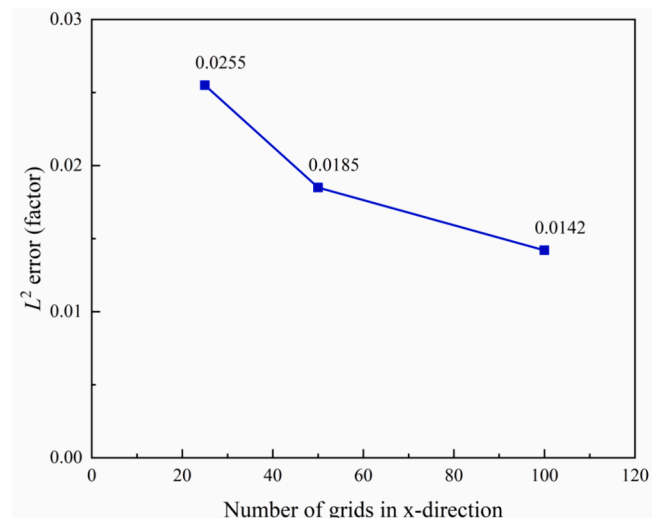


Fig. 5. L^2 absolute errors for different numbers of grids.

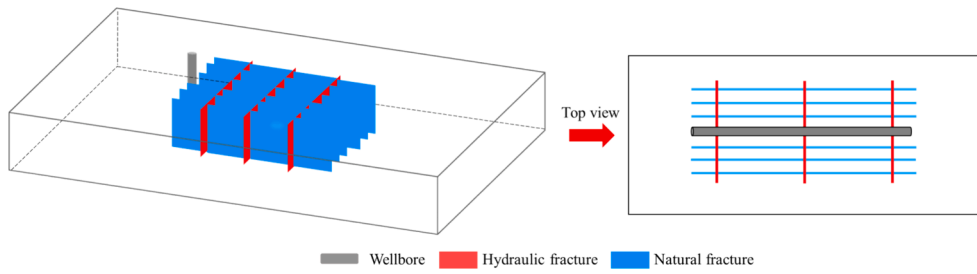
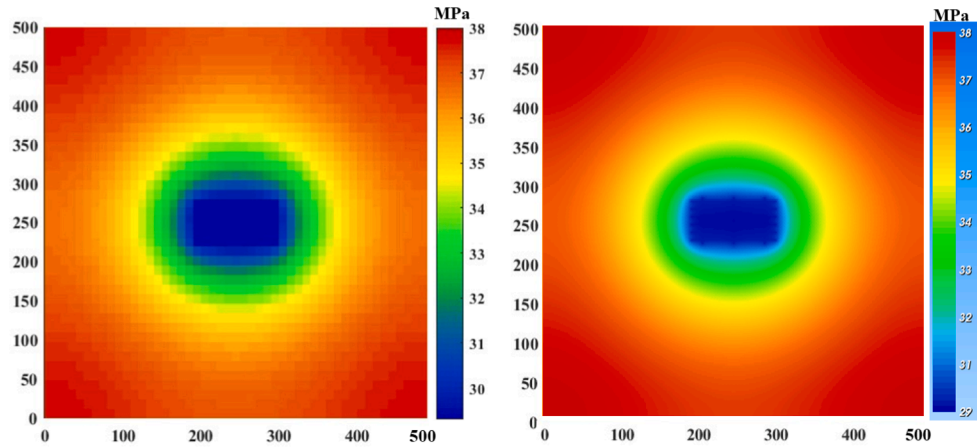


Fig. 6. Schematic diagram of the physical model for model verification.



(a) Pressure distribution in AEDFM. (b) Pressure distribution in KAPPA.

Fig. 7. Pressure distribution in AEDFM and KAPPA simulations.

linear flow, elliptical flow, pseudo-radial flow, and boundary-dominated flow. The pressure derivative slopes for various flow stages, including wellbore storage, bilinear flow, linear flow, elliptical flow, pseudo-radial flow, and boundary-dominated flow, are 1, 1/4, 1/2, 1/3, 0, and 1, respectively. These flow stages have been extensively studied by scholars, and further details can be found in their work (He et al., 2016;

Liu et al., 2020).

To demonstrate the computational advantage of AEDFM, we conducted simulations for cases with 50 grids in the x-direction and 25 grids in the x-direction, respectively. Fig. 4 shows the effect of the number of grids in the x-direction on the pressure and pressure derivative curves. The L^2 absolute error compared to KAPPA's dimensionless pressure for

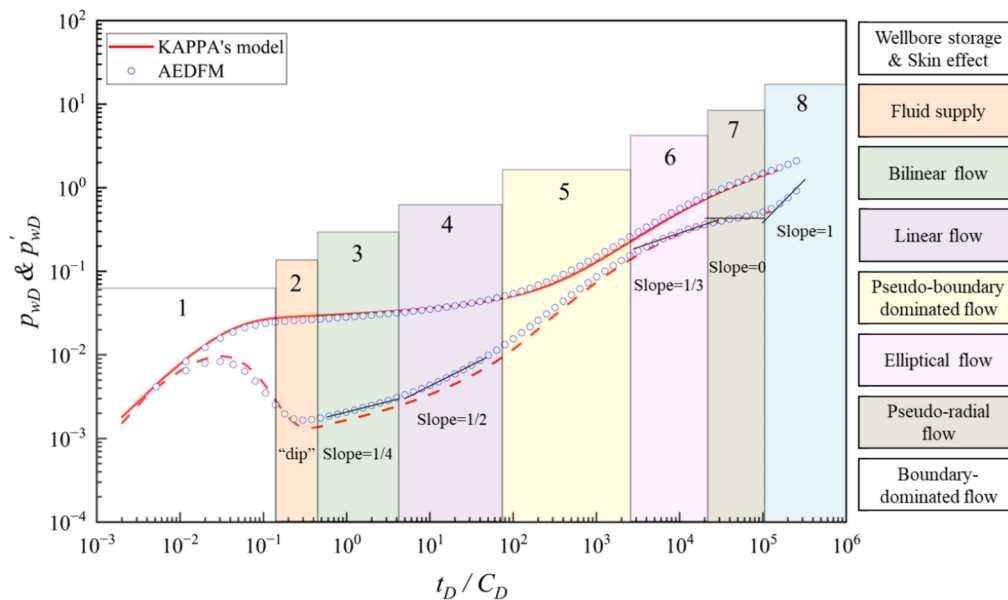


Fig. 8. Comparison between AEDFM and KAPPA's numerical model of Case II.

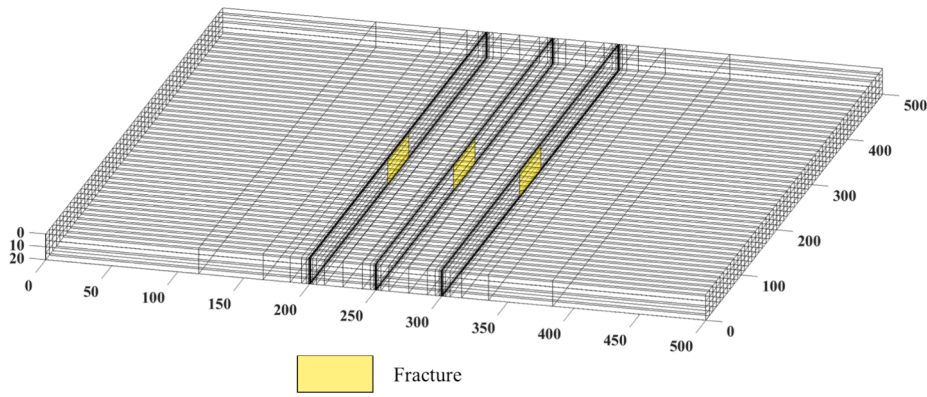


Fig. 9. Locally refined Cartesian grids.

different grid numbers for 25, 50, and 100 grids in the x-direction is given in Fig. 5. The computational error is less than 0.0255, particularly when there are 100 grids in the x-direction, the computational error is 0.0142. Based on Fig. 4 and Fig. 5, it is evident that the number of grids in the x-direction has less impact on the computational results.

Table 2 shows that when AEDFM with only 25 grids in the x-direction has a total of 634 grids in the model, resulting in a computational time that is only 40 % of KAPPA’s model. Increasing the number of grids in the x-direction for AEDFM from 25 to 50 only resulted in a 0.2-second increase in computational time. Furthermore, to ensure computational accuracy and reduce costs, local grid refinement can be implemented near the fractures, while larger grids can be used in areas distant from the fractures. In the Results and Discussion section, we will further demonstrate the advantages of AEDFM by considering different cases.

2.4.2. Case II: With natural fractures

A numerical model with natural fractures is constructed for model verification. The limitations of version 5.20 of KAPPA has that make it challenging to perform local grid refinement around hydraulic fractures when simulating naturally distributed fractures, which can result in errors in the early stages. Therefore, to validate the reliability of AEDFM in a simplified manner, a case involving natural fractures orthogonal to hydraulic fractures is set up, as illustrated in Fig. 6. The input parameters are shown in Table 1. Fig. 7 shows the pressure distribution in both AEDFM and KAPPA, which indicates consistency between their results.

The fact that colormaps in AEDFM and KAPPA are not entirely identical, coupled with their different grid sizes, could explain the visible differences. When simulating natural fractures, KAPPA cannot construct the refined grid shown in Fig. 2b. To ensure accurate results, the KAPPA model uses a fine grid with close to 80,000 grids, while AEDFM only uses 2142 grids. The pressure and pressure derivative curves in Fig. 8 indicate that the results from AEDFM closely match those from KAPPA, with consistent fluid flow regimes despite some differences in values during the middle stage. Thus, the results confirm the reliability of the proposed AEDFM. The flow stages of the MFHW with natural fractures are similar to those of the MFHW without natural fractures. However, the MFHW with natural fractures exhibits a deeper “dip” in the pressure derivative curve compared to the MFHW case without natural fractures. Therefore, the second flow regime is defined as the “fluid supply” stage.

3. Results and discussions

3.1. Limitation of standard EDFM

To demonstrate the superiority of AEDFM, we compared its results with those of the standard EDFM and tEDFM using the parameters of Case I in Table 1. The comparison between the results of our model and those of the analytical model is shown in Fig. 3. Fig. 10 shows that the results of the standard EDFM and tEDFM match those of the analytical model in the late stage. However, their accuracy is lower in the early and

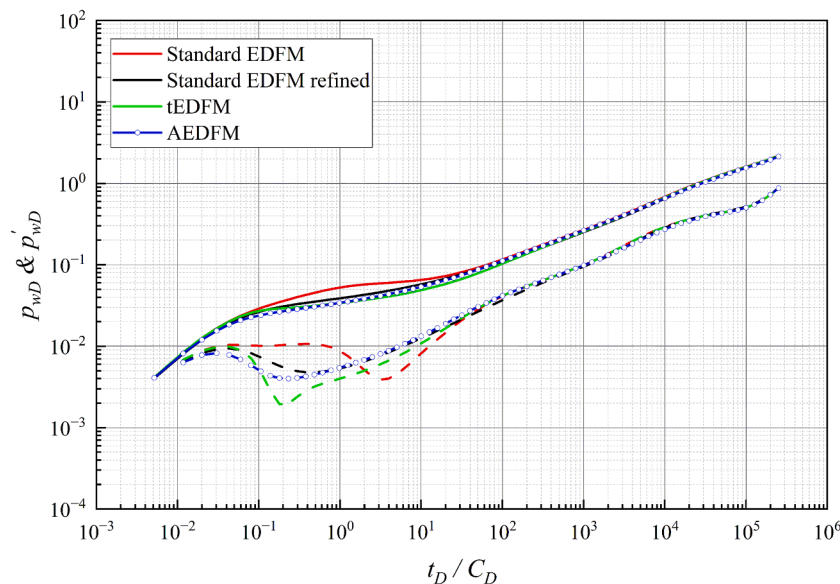
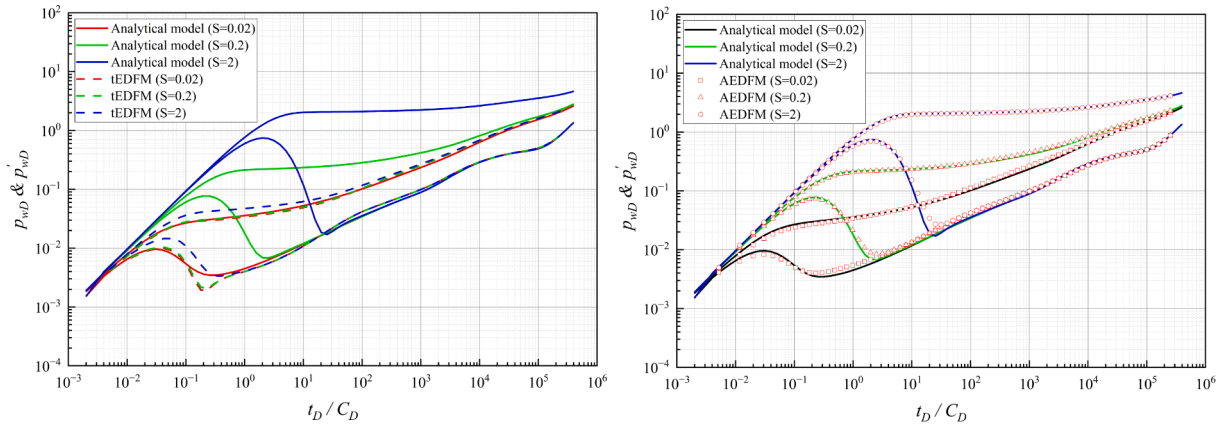


Fig. 10. Comparison between AEDM, EDFM, and tEDFM.



(a) Comparison between the analytical model and tEDFM. (b) comparison between the analytical model and AEDFM.

Fig. 11. Effects of skin coefficient on pressure transient behaviors of fluid flow.

middle stages. As mentioned, the coupling term for flow between the matrix and fractures in EDFM is derived based on the pseudo-steady-state flux assumption. Therefore, it cannot effectively handle the expected early nonlinear pressure drop, resulting in a mismatch in the pressure and pressure derivative curves. By using the locally refined grid shown in Fig. 9, the standard EDFM results show a significant improvement, but errors still exist in the early stages. Additionally, using local grid refinement increases the computational cost and makes it difficult to deal with the case of non-parallel fractures. As depicted in Fig. 10, it can be observed that the tEDFM proposed by Olorode and Rashid (2022) outperforms the standard EDFM, although it is not entirely precise. The reason is that they both used the well index (shown in Eq. (4)) to calculate the fluid flow rates into the wellbore. This wellbore index is derived based on the steady-state assumption, which may introduce inaccuracies at early times. These inaccuracies are visible in the pressure derivative plots shown in Fig. 10.

3.2. Sensitivity analysis.

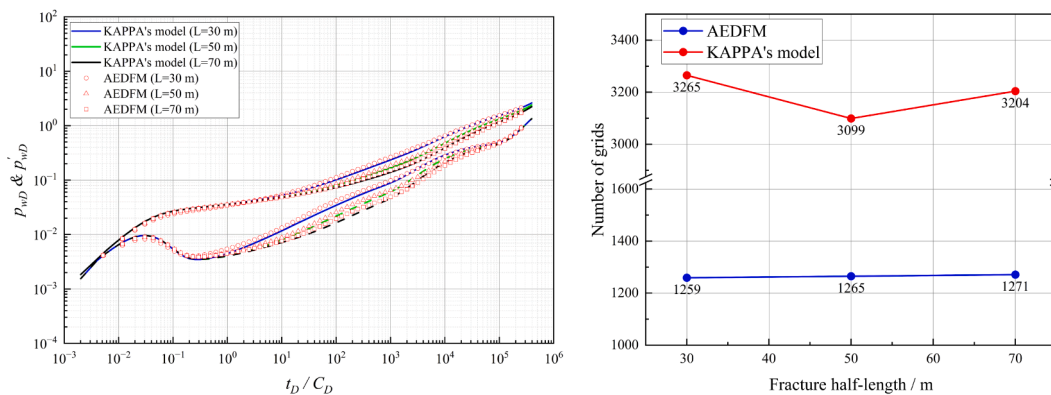
This section investigates the effects of critical parameters, such as skin coefficient and fracture length, on the pressure transient behaviors of fluid flow. Additionally, the advantages of AEDFM are further demonstrated by comparing different cases. The fundamental model parameters for the sensitivity analysis section are presented in Table 1.

3.2.1. Effects of skin coefficient

Fig. 11a illustrates the pressure transient behaviors of fluid flow at various skin coefficients using the tEDFM and an analytical model. The results indicate that the pressure transient behaviors of fluid flow modeled using tEDFM exhibit little change when the skin coefficient changes over two orders of magnitude (from 0.02 to 2). The reason for this is that tEDFM still uses the well index, as shown in Eq. (4), to calculate the flow from the reservoir to the well. This makes it difficult to match the early pressure transient behaviors. In contrast, the analytical model shows that the skin coefficient significantly affects the pressure and pressure derivative curves. The skin coefficient primarily affects the flow regime of “wellbore storage and skin effect”, and the height of the “hump” in the pressure derivative curve is related to $C_D e^{2S}$. This implies that the “hump” becomes higher as the skin coefficient increases. The skin effect causes an additional pressure drop, which is reflected in the pressure curve. However, the results of the AEDFM, as shown in Fig. 11b, match the analytical model very well. This demonstrates that the proposed AEDFM meets the accuracy requirements for well-testing interpretation.

3.2.2. Effects of hydraulic fracture (HF) half-length

Fig. 12a shows the pressure transient behaviors of fluid flow in KAPPA’s numerical model and AEDFM at different HF half-lengths. The results show that the HF half-length mainly affects the shape of the pressure and pressure derivative curves in the middle stage. Longer fractures correspond to lower values of the pressure and pressure



(a) Pressure transient behaviors of fluid flow. (b) Number of grids in AEDFM and KAPPA’s model.

Fig. 12. Comparison of AEDFM and KAPPA’s numerical model at different HF half-lengths.

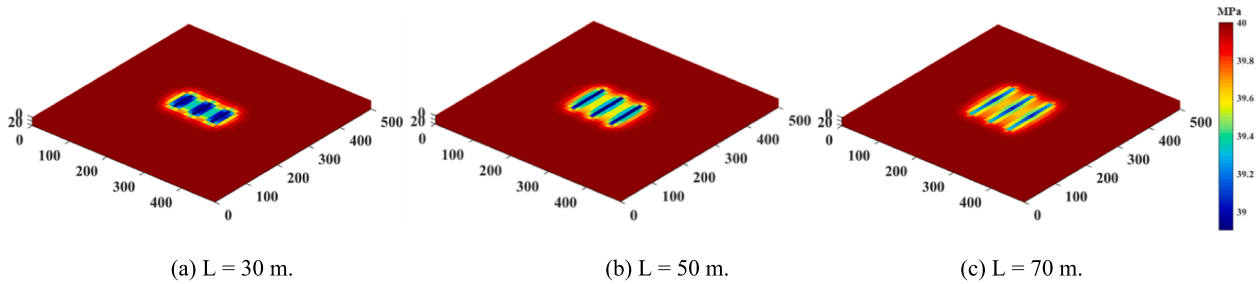


Fig. 13. Pressure distribution map at $t_D/C_D = 200$.

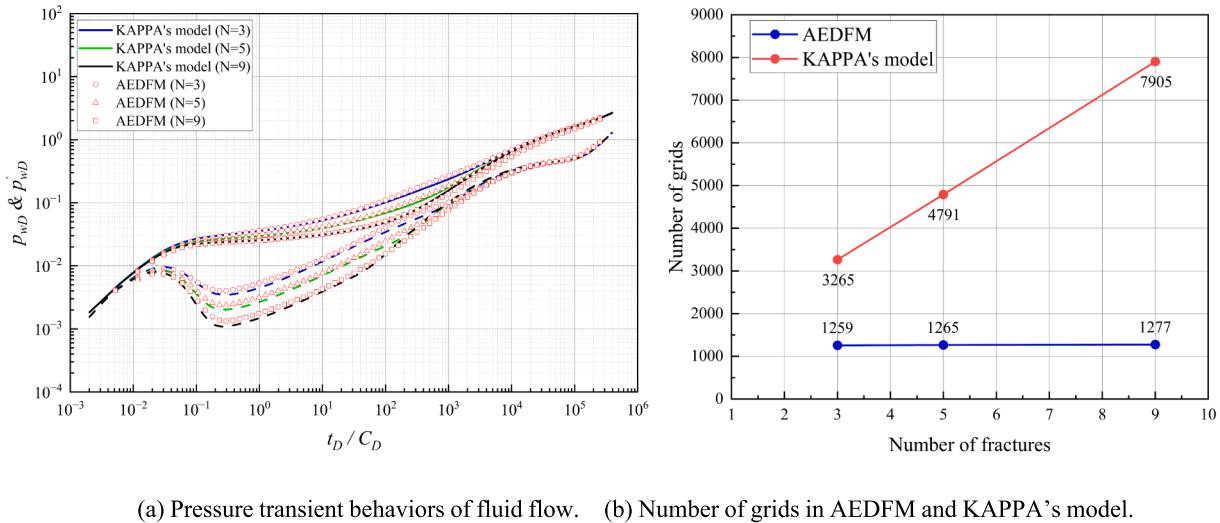


Fig. 14. Comparison of AEDFM and KAPPA's numerical model at different numbers of HF.

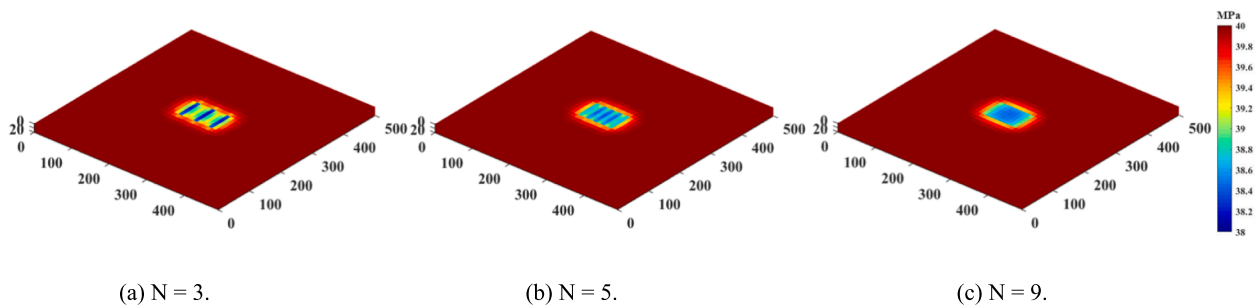


Fig. 15. Pressure distribution map at $t_D/C_D = 200$.

derivative curves. The duration of the bilinear flow stage increases with the length of the hydraulic fracture. From the pressure distribution in Fig. 13, it is more visually apparent that longer fractures result in higher pressure within and around fractures. The results of AEDFM and KAPPA's numerical model are almost identical, with only slight differences in the middle stage, further confirming the accuracy of AEDFM. Fig. 12b compares grid counts between AEDFM and KAPPA's numerical model for cases with different HF lengths. The numerical model grids generated by KAPPA are well-designed, with fewer grids for longer fractures. However, AEDFM utilizes even fewer grids and is more computationally efficient.

3.2.3. Effects of number of hydraulic fractures

The pressure and pressure derivative curves of fluid flow in KAPPA's numerical model and AEDFM at different numbers of HF are plotted in

Fig. 14a. The results show that AEDFM's outcomes match well with those of KAPPA's numerical model. Additionally, the number of HF has a significant impact on pressure and pressure derivative curves in the early and middle stages. Furthermore, an increased number of HF results in a more pronounced "dip" in the pressure derivative curve and a longer duration of bilinear flow. The pressure distribution map in Fig. 15 shows that a greater number of HF leads to higher pressure within the fractures. Fig. 14b compares the grid counts of AEDFM and KAPPA's numerical model, revealing a significant increase in the grid count of KAPPA's numerical model with an increase in the number of HF due to the use of unstructured grids. However, despite the increasing number of HF, the grid count of AEDFM only slightly increases. In the case of an MFHW with nine HF, the number of grids in AEDFM is only 16% of the number of grids in KAPPA's numerical model. As the number of HF increases, AEDFM proves to be more advantageous in terms of the

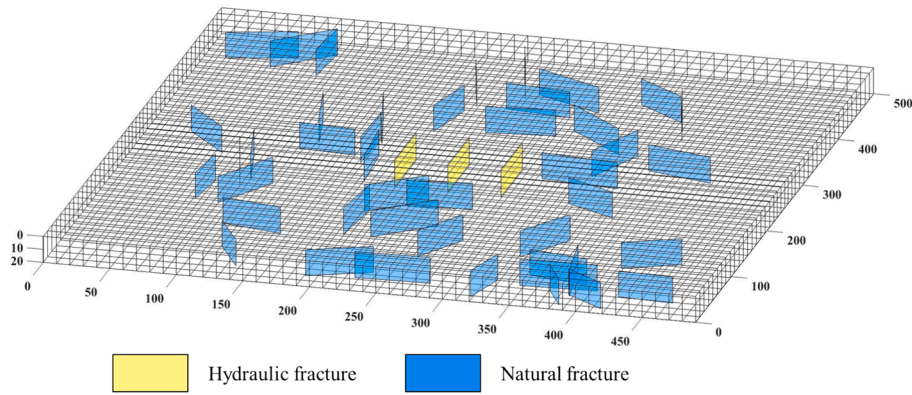


Fig. 16. The grid of AEDFM with discretely distributed natural fractures.

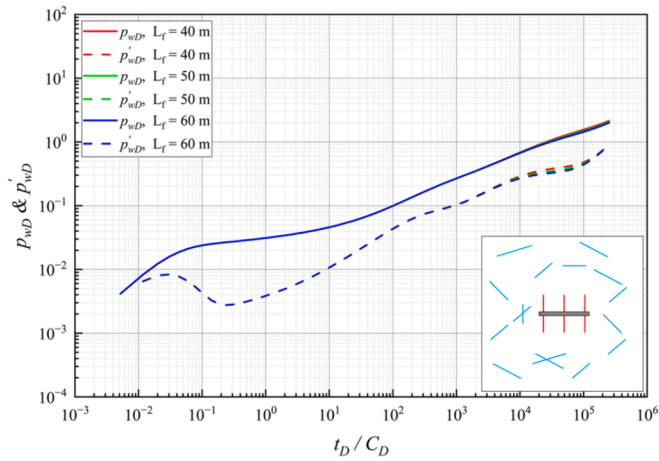


Fig. 17. Effects of average length of NFs on transient pressure behaviors.

number of grids and computational cost.

3.2.4. Effects of natural fracture (NF) half-length.

Fig. 16 shows the grid of AEDFM with discretely distributed natural fractures. The position of natural fractures has a significant impact on the pressure-transient behaviors of fluid flow. To minimize this impact, no natural fractures are added within 30 m of the hydraulic fractures. We investigated the impact of varying average lengths of NFs (namely, 40, 50, and 60 m) on transient pressure behaviors, as shown in Fig. 17.

The pressure distribution at different average lengths of NFs is illustrated in Fig. 18. The results indicate that longer average lengths of NFs lead to lower pressure derivative values at late times. Additionally, longer average lengths of NFs result in higher bottom-hole pressure and the pressure around the wellbore.

3.2.5. Effects of the number of natural fractures

Fig. 19 illustrates the effect of the number of NFs (namely, 10, 20, and 50) on the pressure transient behaviors of fluid flow. As with the

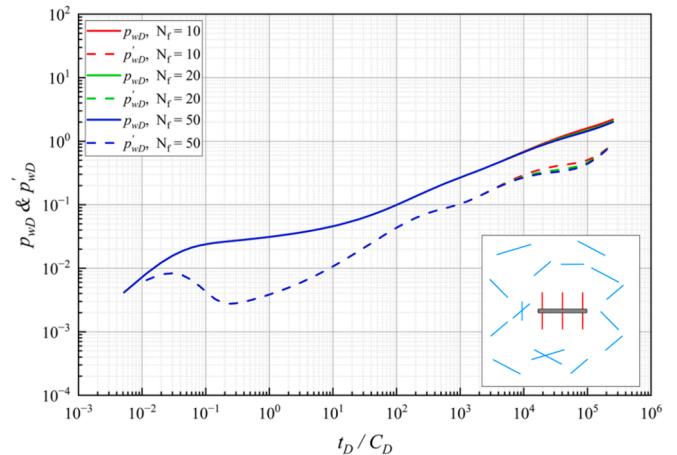
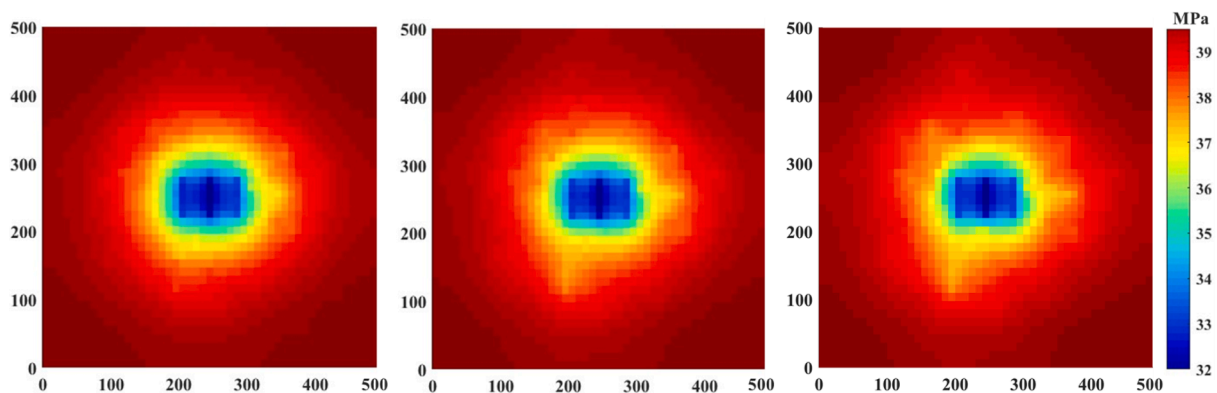


Fig. 19. Effects of number of NFs on transient pressure behaviors.



(a) $L_f = 40$ m.

(b) $L_f = 50$ m.

(c) $L_f = 60$ m.

Fig. 18. Pressure distribution map at $t_D/C_D = 3 \times 10^5$ under different average lengths of NFs.

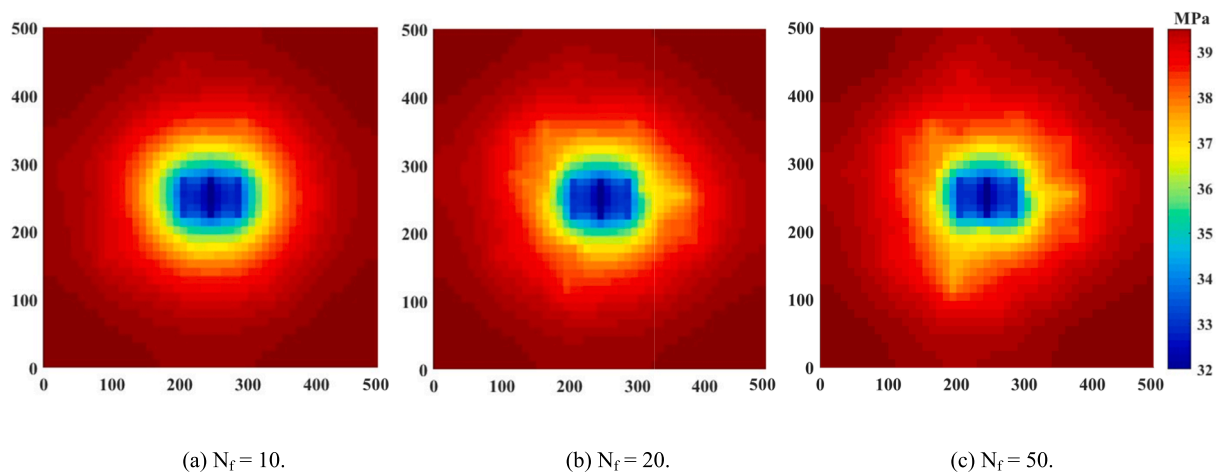


Fig. 20. Pressure distribution map $att_D/C_D = 3 \times 10^5$ under different numbers of NFs.

average lengths of NFs on the pressure transient behaviors, the values of the pressure derivatives decrease in the late stage and the bottom-hole pressure increases as the number of NFs increases. The pressure distribution maps in Fig. 20 show that the pressure propagation range widens as the number of NFs increases. Additionally, the pressure surrounding hydraulic fractures also increases.

It is concluded that in this work, hydraulic fractures mainly affect the pressure transient behaviors of fluid flow during the early and middle stages, while natural fractures mainly affect the pressure transient behaviors during late times. Additionally, the distance between NFs and HF has a significant impact on the transient pressure behaviors of fluid flow. The impact of the number and length of NFs on the pressure transient behaviors of fluid flow is unclear when the number and length of NFs are changed, as this unavoidably affects the relative positions with HF. Therefore, in this work, we have refrained from adding NFs within 30 m of the HF.

4. Conclusions

In this work, we propose a new analytically modified Embedded Discrete Fracture Model (AEDFM) for pressure transient analysis of fluid flow in naturally fractured porous media. The model uses structured Cartesian grids, which significantly reduces computational costs. The main conclusions are as follows:

AEDFM is established by correcting the transmissibility between the matrix and fractures of the standard EDFM through the multiplication of a transient factor. The results show that the AEDFM's results are in good agreement with those of the analytical and high-resolution numerical models.

AEDFM can accurately capture the early transient flow around hydraulic and natural fractures, including early nonlinear pressure drop, which standard EDFM struggles to capture.

AEDFM with structured grids can significantly reduce computational time compared to numerical models that use DFM and unstructured grids with local grid refinement. In the case of only three fractures, the computational time of AEDFM is only 40 % of that of DFM. In cases with more fractures, AEDFM has even greater advantages.

The duration of bilinear flow increases as the length of hydraulic fractures increases. Furthermore, an increase in the number of hydraulic fractures leads to a more pronounced concavity in the pressure derivative curve. Moreover, as the natural fractures become longer and more numerous, the pressure derivative values observed in the late stages decrease.

This study assumes that the fractures are vertical and fully penetrate

the formation. However, fractures in the subsurface could be inclined. Although this is our initial work on using AEDFM for pressure transient analysis, further work will be done to consider the effects of complex fracture geometries and multiphase flow on pressure transient behaviors of fluid flow.

CRedit authorship contribution statement

Biao Zhou: Writing – original draft, Methodology, Conceptualization. **Zhiming Chen:** Writing – review & editing, Methodology, Conceptualization. **Zhigang Song:** Writing – original draft, Methodology, Conceptualization. **Zekai Tang:** Validation, Software, Methodology. **Bin Wang:** Supervision, Software, Methodology. **Olufemi Olorode:** Writing – review & editing, Supervision, Methodology.

Declaration of competing interest

The authors declare that they have no known competing financial interests or personal relationships that could have appeared to influence the work reported in this paper.

Data availability

Data will be made available on request.

Acknowledgment

We are very grateful to all those who have helped to improve this work. It was supported by the Beijing Natural Science Foundation (3232027), the Beijing Nova Program (20230484249), and the National Natural Science Foundation of China (52274046, 52074322 and 52341401). We would like to express our sincere appreciation to the Computational Geosciences group at SINTEF Digital for generously providing the open-source software package, MRST. There is no conflict of interest for any author that is not apparent from the affiliations or funding.

References

- Al-Kobaisi, M., Ozkan, E., Kazemi, H., 2006. A hybrid numerical/analytical model of a finite-conductivity vertical fracture intercepted by a horizontal well. *SPE Reserv. Eval. Eng.* 9 (04), 345–355. <https://doi.org/10.2118/92040-pa>.
- Azom, P.N., Javadpour, F., 2012. Dual-continuum modeling of shale and tight gas reservoirs. *SPE Annual Technical Conference and Exhibition*. <https://doi.org/10.2118/159584-ms>.
- Barenblatt, G.I., Zheltov, I.P., Kochina, I., 1960. Basic concepts in the theory of seepage of homogeneous liquids in fissured rocks. *J. Appl. Math. Mech.* 24 (5), 1286–1303.

- Cao, R., Shi, J., Jia, Z., et al., 2023. A modified 3D-EDFM method considering fracture width variation due to thermal stress and its application in enhanced geothermal system. *J. Hydrol.* 623, 129749 <https://doi.org/10.1016/j.jhydrol.2023.129749>.
- Chandra, V., Corbett, P.W.M.W.M., Geiger, S., Hamdi, H., 2013. Improving reservoir characterization and simulation with near-wellbore modeling. *SPE Reserv. Eval. Eng.* 16 (02), 183–193. <https://doi.org/10.2118/148104-pa>.
- Chen, Z., Yu, W., 2022. A discrete model for pressure transient analysis in discretely fractured reservoirs. *SPE J.* 27 (03), 1708–1728. <https://doi.org/10.2118/209214-pa>.
- Chen, Z., Zhou, B., Zhang, S., et al., 2023. Pressure transient behaviors for horizontal wells with well interferences, complex fractures and two-phase flow. *Geoenergy Sci. Eng.* 227, 211845 <https://doi.org/10.1016/j.geoen.2023.211845>.
- Dean, R.H., Lo, L.L., 1988. Simulations of naturally fractured reservoirs. *SPE Reserv. Eng.* 3 (02), 638–648. <https://doi.org/10.2118/14110-pa>.
- Egya, D.O., et al., 2019. Analysing the limitations of the dual-porosity response during well tests in naturally fractured reservoirs. *Pet. Geosci.* 25 (1), 30–49. <https://doi.org/10.1144/petgeo2017-053>.
- Gilman, J.R., Kazemi, H., 1983. Improvements in simulation of naturally fractured reservoirs. *SPE J.* 23 (04), 695–707. <https://doi.org/10.2118/10511-pa>.
- He, Y., Cheng, S., Li, S., et al., 2016. A semianalytical methodology to diagnose the locations of underperforming hydraulic fractures through pressure-transient analysis in tight gas reservoir. *SPE J.* 22 (03), 924–939. <https://doi.org/10.2118/185166-pa>.
- Houzé, O., Viturat, D., Fjaere, O.S., 2008. *Dynamic data analysis*. Kappa Engineering, Paris, p. 694.
- Hu, P., Geng, S., Liu, X., et al., 2023. A three-dimensional numerical pressure transient analysis model for fractured horizontal wells in shale gas reservoirs. *J. Hydrol.* 620, 129545 <https://doi.org/10.1016/j.jhydrol.2023.129545>.
- Jiang, J., Younis, R.M., 2015. Numerical study of complex fracture geometries for unconventional gas reservoirs using a discrete fracture-matrix model. *J. Nat. Gas Sci. Eng.* 26, 1174–1186. <https://doi.org/10.1016/j.jngse.2015.08.013>.
- Karimi-Fard, M., Firoozabadi, A., 2001. Numerical simulation of water injection in 2D fractured media using discrete-fracture model. *SPE Annual Technical Conference and Exhibition*. <https://doi.org/10.2118/71615-ms>.
- Karimi-Fard, M., Firoozabadi, A., 2003. Numerical simulation of water injection in fractured media using the discrete-fracture model and the galerkin method. *SPE Reserv. Eval. Eng.* 6 (02), 117–126. <https://doi.org/10.2118/83633-pa>.
- Kazemi, H., Merrill Jr., L.S., Porterfield, K.L., Zeman, P.R., 1976. Numerical simulation of water-oil flow in naturally fractured reservoirs. *SPE J.* 16 (06), 317–326. <https://doi.org/10.2118/5719-pa>.
- Kim, J.-G., Deo, M.D., 2000. Finite element, discrete-fracture model for multiphase flow in porous media. *AIChE J.* 46 (6), 1120–1130. <https://doi.org/10.1002/aic.690460604>.
- Kuchuk, F., Biryukov, D., 2014. Pressure-transient behavior of continuously and discretely fractured reservoirs. *SPE Reserv. Eval. Eng.* 17 (01), 82–97. <https://doi.org/10.2118/158096-pa>.
- Lee, S.H., Lough, M.F., Jensen, C.L., 2001. Hierarchical modeling of flow in naturally fractured formations with multiple length scales. *Water Resour. Res.* 37 (3), 443–455. <https://doi.org/10.1029/2000WR900340>.
- Li, L., Lee, S.H., 2008. Efficient field-scale simulation of black oil in a naturally fractured reservoir through discrete fracture networks and homogenized media. *SPE Reserv. Eval. Eng.* 11 (04), 750–758. <https://doi.org/10.2118/103901-pa>.
- Lie, K.-A., 2019. An introduction to reservoir simulation using MATLAB/GNU octave: user guide for the MATLAB Reservoir Simulation Toolbox (MRST). Cambridge University Press. <https://doi.org/10.1017/9781108591416>.
- Lie, K.-A., Møyner, O., 2021. *Advanced modelling with the MATLAB reservoir simulation toolbox*. Cambridge University Press. <https://doi.org/10.1017/9781009019781>.
- Liu, H., Zhao, X., Tang, X., et al., 2020. A discrete fracture-matrix model for pressure transient analysis in multistage fractured horizontal wells with discretely distributed natural fractures. *J. Pet. Sci. Eng.* 192, 107275 <https://doi.org/10.1016/j.petrol.2020.107275>.
- Liu, H., Liao, X., Zhao, X., et al., 2022. A high-resolution numerical well-test model for pressure transient analysis of multistage fractured horizontal wells in naturally fractured reservoirs. *J. Pet. Sci. Eng.* 208, 109417 <https://doi.org/10.1016/j.petrol.2021.109417>.
- Moinfar, A., Varavei, A., Sepehrnoori, K., Johns, R.T., 2013. Development of an efficient embedded discrete fracture model for 3D compositional reservoir simulation in fractured reservoirs. *SPE J.* 19 (02), 289–303. <https://doi.org/10.2118/154246-pa>.
- Olorode, O., Rashid, H., 2022. Analytical modification of EDFM for transient flow in tight rocks. *Sci. Rep.* 12 (1), 22018. <https://doi.org/10.1038/s41598-022-26536-w>.
- Olorode, O., Wang, B., Rashid, H.U., 2020. Three-dimensional projection-based embedded discrete-fracture model for compositional simulation of fractured reservoirs. *SPE J.* 25 (04), 2143–2161. <https://doi.org/10.2118/201243-PA>.
- Peaceman, D., 1983. Interpretation of well-block pressures in numerical reservoir simulation with nonsquare grid blocks and anisotropic permeability. *SPE J.* 23 (03), 531–543. <https://doi.org/10.2118/10528-PA>.
- Pruess, K., Narasimhan, T.N., 1985. A practical method for modeling fluid and heat flow in fractured porous media. *SPE J.* 25 (01), 14–26. <https://doi.org/10.2118/10509-pa>.
- Pruess, K., Wu, Y.-S., 1993. A new semi-analytical method for numerical simulation of fluid and heat flow in fractured reservoirs. *SPE Adv. Technol. Ser.* 1 (02), 63–72. <https://doi.org/10.2118/18426-pa>.
- Rashid, H.U., Olorode, O., 2023. A continuous projection-based EDFM model for flow in fractured reservoirs. *SPE J.* 29 (01), 476–492. <https://doi.org/10.2118/217469-PA>.
- Sandve, T.H., Berre, I., Nordbotten, J.M., 2012. An efficient multi-point flux approximation method for discrete fracture-matrix simulations. *J. Comput. Phys.* 231 (9), 3784–3800. <https://doi.org/10.1016/j.jcp.2012.01.023>.
- Ṭene, M., Bosma, S.B.M., Al Kobaisi, M.S., Hajibeygi, H., 2017. Projection-based Embedded Discrete Fracture Model (pEDFM). *Adv. Water Resour.* 105, 205–216. <https://doi.org/10.1016/j.advwatres.2017.05.009>.
- Vermeulen, T., 1953. Theory for irreversible and constant-pattern solid diffusion. *Ind. Eng. Chem.* 45 (8), 1664–1670. <https://doi.org/10.1021/ie50524a025>.
- Vinsome, P.K.W., Westerveld, J., 1980. A simple method for predicting cap and base rock heat losses in thermal reservoir simulators. *J. Can. Pet. Technol.* 19 (03) <https://doi.org/10.1016/j.advwatres.2017.05.009>.
- Wan, J., Aziz, K., 1999. Multiple hydraulic fractures in horizontal wells. *SPE Western Regional Meeting*. <https://doi.org/10.2118/54627-ms>.
- Wang, B., Fidelibus, C., 2021. An open-source code for fluid flow simulations in unconventional fractured reservoirs. *Geosciences* 11 (2), 106. <https://doi.org/10.3390/geosciences11020106>.
- Warren, J.E., Root, P.J., 1963. The behavior of naturally fractured reservoirs. *SPE J.* 3 (03), 245–255. <https://doi.org/10.2118/426-pa>.
- Wu, K., Wu, B., Yu, W., 2017. Mechanism analysis of well interference in unconventional reservoirs: insights from fracture-geometry simulation between two horizontal wells. *SPE Prod. Oper.* 33 (01), 12–20. <https://doi.org/10.2118/186091-pa>.
- Xiang, Z., Zhen, R., Xu, Y., et al., 2023. A numerical pressure transient model of fractured well with complex fractures of tight gas reservoirs considering gas-water two phase by EDFM. *Geoenergy Sci. Eng.* 231, 212286 <https://doi.org/10.1016/j.geoen.2023.212286>.
- Xu, Y., Sepehrnoori, K., 2022. Modeling fracture transient flow using the embedded discrete fracture model with nested local grid refinement. *J. Pet. Sci. Eng.* 218, 110882 <https://doi.org/10.1016/j.petrol.2022.110882>.
- Xu Y. (2015). Implementation and application of the embedded discrete fracture model (EDFM) for reservoir simulation in fractured reservoirs. <http://hdl.handle.net/2152/34216>.
- Yu, W., Xu, Y., Weijermars, R., Wu, K., Sepehrnoori, K., 2017. A numerical model for simulating pressure response of well interference and well performance in tight oil reservoirs with complex-fracture geometries using the fast embedded-discrete-fracture-model method. *SPE Reserv. Eval. Eng.* 21 (02), 489–502. <https://doi.org/10.2118/184825-pa>.
- Yu, W., Zhang, Y., Varavei, A., et al., 2019. Compositional simulation of CO₂ Huff 'n' puff in eagle ford tight oil reservoirs with CO₂ molecular diffusion, nanopore confinement, and complex natural fractures. *SPE Reserv. Eval. Eng.* 22 (02), 492–508. <https://doi.org/10.2118/190325-pa>.
- Zhan, W., Zhao, H., Rao, X., et al., 2023. Generalized finite difference method-based numerical modeling of oil-water two-phase flow in anisotropic porous media. *Phys. Fluids* 35, 103317. <https://doi.org/10.1063/5.0166530>.
- Zhao, X., Chen, Z., Wang, B., et al., 2023. A Multi-medium and Multi-mechanism model for CO₂ injection and storage in fractured shale gas reservoirs. *Fuel* 345, 128167. <https://doi.org/10.1016/j.fuel.2023.128167>.
- Zhao, L., Jiang, H., Zhang, S., et al., 2018. Modeling vertical well in field-scale discrete fracture-matrix model using a practical pseudo inner-boundary model. *J. Pet. Sci. Eng.* 166, 510–530. <https://doi.org/10.1016/j.petrol.2018.02.061>.
- Zimmerman, R.W., Chen, G., Hadgu, T., Bodvarsson, G.S., 1993. A numerical dual-porosity model with semianalytical treatment of fracture/matrix flow. *Water Resour. Res.* 29 (7), 2127–2137. <https://doi.org/10.1029/93WR00749>.